Orientation Dynamics of Main-Chain Liquid Crystal Polymers. 2. Structure and Kinetics in a Magnetic Field

J. S. Moore and S. I. Stupp*

Polymer Group, College of Engineering, University of Illinois at Urbana-Champaign, Urbana, Illinois 61801. *Received June 16, 1986*

ABSTRACT: Several aspects of molecular organization and dynamics in liquid crystal polymers have been revealed by orientation kinetics in a magnetic field. The technique used was pulsed broad-line proton NMR, and the polymers were liquid crystal copolymers synthesized in our laboratory. Interestingly, isothermal aging before application of the magnetic field leads to a drastic reduction in orientation time, reflecting the nonequilibrium nature of the mesophase structure. The fitting of data to a theoretical model of the orientation process plus other observations leads to the following conclusions. The liquid crystal fluid either is multiphasic or contains an interphase region in which chain segments have greater mobility and perhaps less order. At least for samples in nonequilibrium states, experimental results could be consistent with segments of a single chain traversing various orientationally ordered domains. This type of molecular organization may be viewed as a liquid fringed micelle.

Introduction

Many aspects of the structure and molecular dynamics of liquid crystal polymers (LCP's) remain unknown. It is clear at this point that our understanding of monomer-sized liquid crystal molecules is not fully transferrable to polymers. Peculiar behavior in LC polymers is continuously being reported as more laboratories make contributions in this field. The technological importance of this area of research is based on the potential of self-ordering behavior in producing advanced materials.

A most interesting feature of LC phases is their facile molecular reorientation by weak external fields. In small-molecule liquid crystals this phenomenon can occur in time scales under a second in either electric[1] or magnetic fields.[2] This reorientation in a magnetic field is schematically illustrated in Figure 1, which shows realignment of the director axis, $\vec{n}$, in a monodomain or polydomain sample. In contrast to the rapid response of small molecules, one might intuitively expect much longer reorientation times in polymeric liquid crystals. The controlling variables and limits of such realignment kinetics should be most informative on the equilibrium structure and dynamics of the liquid mesophase. Furthermore, the process of realignment offers interesting possibilities in a materials science context. One is the physical synthesis of phases crystallized or solidified under the influence of the reorienting field, and in this regard kinetics become a critical factor. Furthermore, solidification of the aligned mesophase is of interest to study properties of highly ordered or anisotropic materials. In small-molecule liquid crystals this opportunity is not readily apparent since formation of an unoriented polycrystalline microstructure is inevitable when the oriented fluid solidifies. The greater possibilities for oriented materials using polymer liquid crystals are based on slower crystallization and/or longer relaxation times. Oriented solids may also be possible due to inhibited crystallization in chemically disordered backbones.

Over the past few years several research groups have reported macroscopic orientation of polymer liquid crystals (PLC's) by magnetic fields.[3-11] One observation common to these studies is that the rate of orientation is much slower in polymers compared to that in their small-molecule counterparts. Molecular weight and therefore melt viscosity have been considered important variables in magnetic alignment of PLC's. For example, Martins et al.[3] were able to easily orient a low molecular weight polymer in a field of 1.2 T. On the other hand, the high molecular weight analogue of the same polymer showed no sign of macroscopic alignment in this same field over a period of 1 h. In another example, Hardouin et al.[4] studied the effects of melt viscosity on orientation. It was found that the threshold field strength required to achieve alignment increased with the melt viscosity. Very little information is presently available on the details of orientation kinetics, including quantitative analysis and the control of molecular and thermal history variables. It is this kind of information that is necessary for a fundamental understanding of structure in the polymeric mesophase and its cooperative behavior.

We report here our studies on the orientation kinetics of a main-chain liquid crystal polymer in a magnetic field. The samples used in the study were mesogenic polyesters synthesized and characterized in our laboratory. We have described this aspect of our work in the first paper of this series. The general structure for the experimental polymer is that shown in 1. As pointed out in the previous paper,

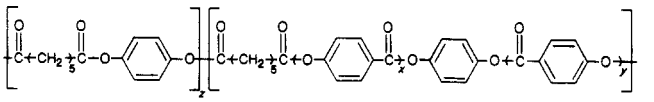

1

$x \geq 0, y \geq 0$

$x + y \geq 1, z = x + y - 1$

transesterification does occur during polymerization and the chain can be described as one having a random sequence of structural units. In the present study we have used Fourier transform broad-line proton NMR to measure macroscopic order as a function of time under the influence of a magnetic field of 4.7 T. The variables of interest have been molecular weight, temperature, and the isothermal aging time of the mesophase prior to magnetic alignment.

Experimental Section

The synthesis and characterization of the experimental polymers was described earlier.[12] Samples were prepared in standard 5-mm-diameter NMR tubes, which were filled with 0.4 g of polymer added in five equal-mass portions. After the addition of each portion, the tube was heated to 200 °C for 2 min and then packed lightly with a solid glass rod. Once the tube had been filled, it was evacuated, filled with dry nitrogen gas, and heated to 200 °C for a period of 60 min. This time was only varied in experiments studying the effect of isothermal aging.

Proton NMR measurements were obtained with a Varian XL-200 instrument equipped with a variable-temperature unit. Once in place within the NMR instrument, all samples were heated to 140 °C and kept at this temperature for 5.0 min before

0024-9297/87/2220-0282$01.50/0

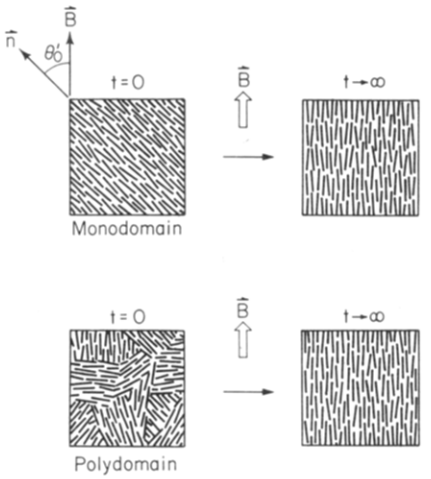

Figure 1. Schematic representation of magnetic alignment experiments. The top diagram illustrates reorientation of a monodomain sample in which the director makes an initial angle θ_0' with respect to the external field. The bottom diagram illustrates macroscopic alignment of a polydomain sample having random orientation at $t = 0$.

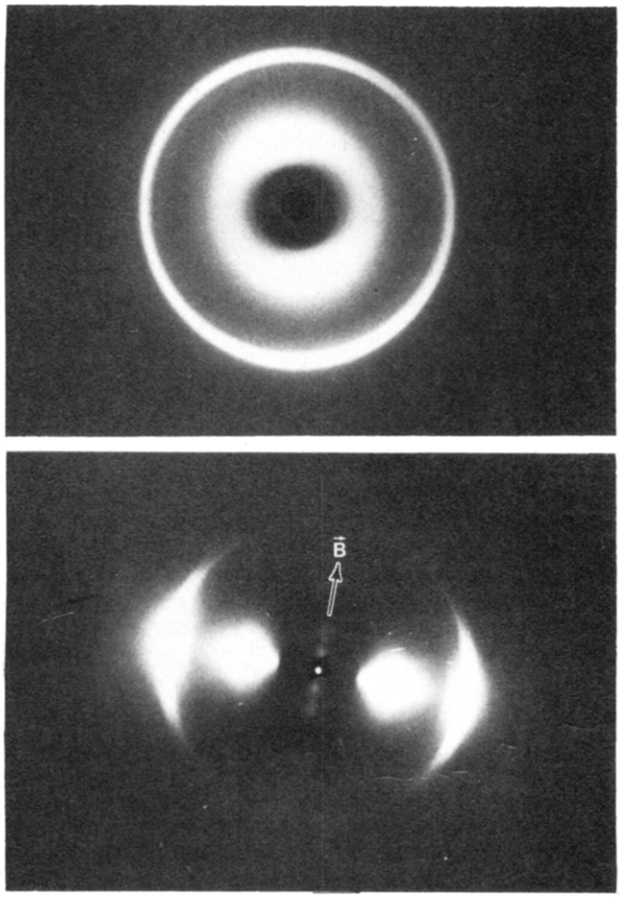

Figure 2. X-ray photographs of experimental polyester solidified from an unoriented mesophase (top) and a magnetically oriented mesophase (bottom).

starting collection of orientation data. At the end of this 5.0-min period, the temperature was increased to that used in the orientation experiment. This stepwise heating program was necessary for two reasons. One was to prevent large temperature overshoots that resulted when heating directly from room temperature. A second reason was to shorten the time involved in melting the samples and thus avoid significant magnetic orientation before reaching the desired temperature. A spectral width of 80 kHz, pulse width of 1.0 μs (90° pulse width = 13 μs), and acquisition time of 100 ms were used for data collection. The

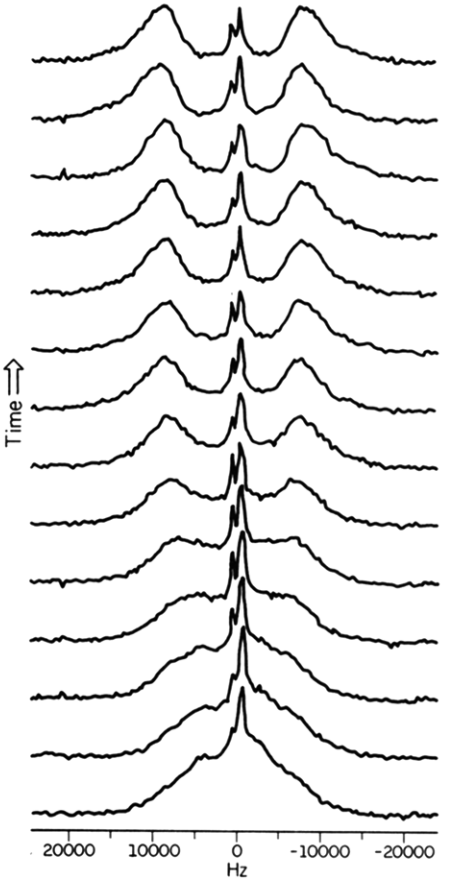

Figure 3. Broad-line ^1H NMR spectra of the experimental polyester in the fluid state with increasing time in the magnetic field (T = 185 °C).

Fourier transformation utilized 256 data points, and the magnetic field and radiation frequency were 4.7 T and 200 MHz, respectively.

Results and Discussion

Data Analysis and General Observations. Figure 2 shows two X-ray photographs of solid polymer samples. One corresponds to a sample obtained after solidification of an unoriented fluid (top). The other photograph corresponds to a sample that was exposed to a magnetic field in the fluid state and solidified in the presence of the field (bottom). The direction of the magnetic field is indicated in the bottom photograph of Figure 2. It is clear that macroscopic molecular orientation is induced by the field and retained after solidification of the sample. One objective of our paper has been to study the kinetics of this field-induced orientation in the fluid state. A second objective has been to characterize from kinetic data and other measurements molecular organization in the mesophase.

Figure 3 shows the gradual change observed in the broad-line NMR spectrum of a liquid crystal sample with time under the influence of a magnetic field. The gradual appearance of two well-defined bands symmetric in frequency above and below the central resonance peak is an indication of macroscopic molecular orientation in the liquid sample. This effect is caused by dipolar interactions between protons in the orientationally ordered fluid.[13] A nonzero order parameter in the liquid causes a splitting of magnetic energy levels, which becomes quite apparent as the macroscopic order parameter of the sample increases. From the proton NMR spectra collected as a function of time we obtained values of the second moment, $\langle \Delta\nu^2 \rangle$, defined as

$$\langle \Delta\nu^2 \rangle = \frac{\int_{-\infty}^{\infty} [\nu - \langle \nu \rangle]^2 g(\nu)\, d\nu}{\int_{-\infty}^{\infty} g(\nu)\, d\nu} \quad (1)$$

where $g(\nu)$ represents the functional form of the NMR line shape, ν is the frequency at which resonance occurs, and $\langle \nu \rangle$ is the average frequency of the resonance band. Since in a classical nematic phase intermolecular dipolar spin interactions are time averaged to zero, theoretical expressions describing the second moment are considerably simplified in comparison to those for the solid phase. We have assumed this to be a reasonable first-order approximation for our system. The theoretical relationship for $\langle \Delta\nu^2 \rangle_M$, the value of the second moment for a single-component liquid crystalline phase is given by

$$\langle \Delta\nu^2 \rangle_M = 3\left(\frac{\gamma^2}{2\pi}\right)^2 h^2 I(I+1) \langle S^2_{z'z'} \rangle \sum_{pq} \frac{1}{r_{pq}^6} [s_{zz} \langle \tfrac{3}{2} \cos^2 \beta_{pq} - \tfrac{1}{2} \rangle + \tfrac{1}{2}(s_{xx} - s_{yy}) \langle \sin^2 \beta_{pq} \cos 2\alpha_{pq} \rangle]^2 \quad (2)$$

where the summation is carried out over all spins p and q ($p \neq q$) of the same nuclei within a given molecule or molecular subunit. The angles α and β are the Eulerian angles relating the p–q internuclear vector to the principal molecular axes, and r_{pq} is the internuclear distance. $S_{z'z'}$ is the macroscopic order parameter, defined as

$$S_{z'z'} = \tfrac{3}{2} \cos^2 \theta_0 - \tfrac{1}{2} \quad (3)$$

where θ_0 is the angle that the macroscopic director makes with the external magnetic field. s_{xx}, s_{yy}, and s_{zz} are the microscopic order parameters, given by

$$s_{zz} = \tfrac{3}{2} \cos^2 \theta - \tfrac{1}{2} \quad (4)$$

$$s_{xx} - s_{yy} = \tfrac{3}{2} \sin^2 \theta \cos 2\Psi \quad (5)$$

The other symbols in eq 2 have their usual meaning. θ in eq 4 and 5 represents the angle between the principal molecular axis and the local director. $\langle s_{zz} \rangle$ and $\langle s_{xx} - s_{yy} \rangle$ reflect the time average of thermal fluctuations of molecules about their local director while $\langle S^2_{z'z'} \rangle$ reflects the spatial average (orientational distribution) of the directors over the entire sample. Since all the time-averaged terms in eq 2 can be assumed to be constant at a given temperature and independent of the macroscopic director orientation, the value of $\langle \Delta\nu^2 \rangle_M$ can be assumed to be directly proportional to $\langle S^2_{z'z'} \rangle$. $\langle S^2_{z'z'} \rangle$ takes on the value of unity in samples uniformly aligned parallel to the external field ($\theta_0 = 0$). Therefore, the ratio of the second moment of an unoriented or partly oriented sample to the second moment of a sample macroscopically aligned with the field is

$$\langle \Delta\nu^2 \rangle_M / \langle \Delta\nu^2 \rangle^0_M = \langle S^2_{z'z'} \rangle \quad (6)$$

Thus, provided $\langle \Delta\nu^2 \rangle^0_M$ is known, monitoring $\langle \Delta\nu^2 \rangle_M$ as a function of time allows us to follow alignment kinetics. The value of $\langle \Delta\nu^2 \rangle^0_M$ can be easily obtained for polymers that achieve complete macroscopic alignment. However, as shown below, the highest molecular weight sample does not acquire full macroscopic alignment under the conditions of the experiment. Therefore, for this particular sample we assume the value of $\langle \Delta\nu^2 \rangle^0_M$ to be equal to that of the sample with slightly lower molecular weight. This is reasonable, considering that $\langle \Delta\nu^2 \rangle^0_M$ did not change significantly over a wide range of molecular weights.

The central sharp peak observed in NMR spectra shown in Figure 3 has been attributed to the presence of an isotropic component that coexists with the uniaxial mesophase.[14] The evidence comes from NMR experiments on deuteriated samples. For convenience in the discussion that follows, we will refer to the central peak as one resulting from the presumed isotropic component. However, we emphasize that we have no direct evidence at this point to claim that this central peak arises from the presence of an optically submicroscopic isotropic component. We return to this point toward the end of the paper and discuss the implications of our data to this issue.

On the basis of the discussion above, the second moment measured from experimental spectra is assumed to have a contribution from an isotropic component. If $A_{\nu 0}/A_t$ corresponds to the molar fraction of material in the isotropic phase with a second moment of $\langle \Delta\nu^2 \rangle_I$ and the value of the second moment of the pure mesophase is given by $\langle \Delta\nu^2 \rangle_M$, then the observed second moment $\langle \Delta\nu^2 \rangle$ can be written as

$$\langle \Delta\nu^2 \rangle = (A_{\nu 0}/A_t)\langle \Delta\nu^2 \rangle_I + (1 - (A_{\nu 0}/A_t))\langle \Delta\nu^2 \rangle_M \quad (7)$$

For those polymer samples that achieve complete alignment, the isotropic component of the most oriented spectrum can be easily resolved from the mesophase component (see top spectrum, Figure 3). Integration of the respective components in this spectrum provides an estimate of $A_{\nu 0}/A_t$, and using the area under the central peak, we have estimated $\langle \Delta\nu^2 \rangle_I$. We have assumed the values of $\langle \Delta\nu^2 \rangle_I$ to be constant throughout the process of alignment in the external field. Knowing $A_{\nu 0}/A_t$ and $\langle \Delta\nu^2 \rangle_I$, we can determine the contribution of the uniaxial mesophase to the second moment, $\langle \Delta\nu^2 \rangle_M$, for all spectra by rearrangement of eq 7, and using the experimentally measured values of the total second moment $\langle \Delta\nu^2 \rangle$, we may write

$$\langle \Delta\nu^2 \rangle_M = \frac{\langle \Delta\nu^2 \rangle - (A_{\nu 0}/A_t)\langle \Delta\nu^2 \rangle_I}{1 - (A_{\nu 0}/A_t)} \quad (8)$$

In a similar manner, we can write the second moment of a fully aligned mesophase as

$$\langle \Delta\nu^2 \rangle^0_M = \frac{\langle \Delta\nu^2 \rangle^0 - (A_{\nu 0}/A_t)\langle \Delta\nu^2 \rangle_I}{1 - (A_{\nu 0}/A_t)} \quad (9)$$

where $\langle \Delta\nu^2 \rangle^0$ is the second moment measured for a completely aligned sample ($\theta_0 = 0$). For experimental polymers that did not achieve complete orientation, $A_{\nu 0}/A_t$ and $\langle \Delta\nu^2 \rangle_I$ were estimated from measurements on lower molecular weight samples. As it turned out, the value of $\langle \Delta\nu^2 \rangle_I$ was found to be about 2 orders of magnitude smaller than $\langle \Delta\nu^2 \rangle$, and hence its contribution to the total second moment was almost negligible.

Substitution of eq 8 and 9 into eq 6 yields

$$\frac{\langle \Delta\nu^2 \rangle - (A_{\nu 0}/A_t)\langle \Delta\nu^2 \rangle_I}{\langle \Delta\nu^2 \rangle^0 - (A_{\nu 0}/A_t)\langle \Delta\nu^2 \rangle_I} = \langle S^2_{z'z'} \rangle \quad (10)$$

We have used this equation to follow the kinetics of alignment in a magnetic field. Since $\langle \Delta\nu^2 \rangle^0$ is defined for a state of complete orientation, it is important that the value assigned to this parameter be obtained with a sample having uniform alignment parallel to the field. In Figure 4 we have plotted typical data of $\langle \Delta\nu^2 \rangle$ as a function of time obtained from spectra shown in Figure 3. The constant value observed for $\langle \Delta\nu^2 \rangle$ after ca. 7000 s suggests that the material has achieved maximum alignment at this point, and hence a value for $\langle \Delta\nu^2 \rangle^0$ can be tentatively obtained from the asymptotic portion of the curve. The sample has no preferred orientation initially, and $\langle S^2_{z'z'} \rangle$ for such a sample should be equal to 0.2. Therefore, the

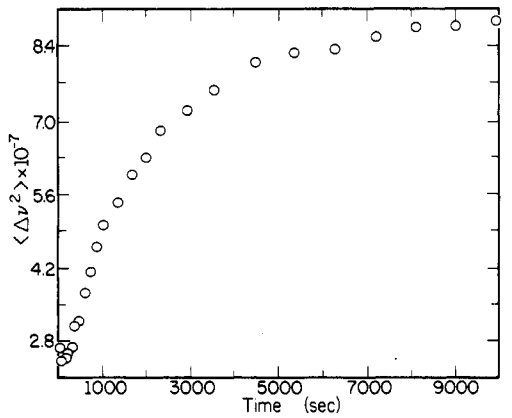

Figure 4. Plot of experimentally measured second-moment values as a function of time in the magnetic field.

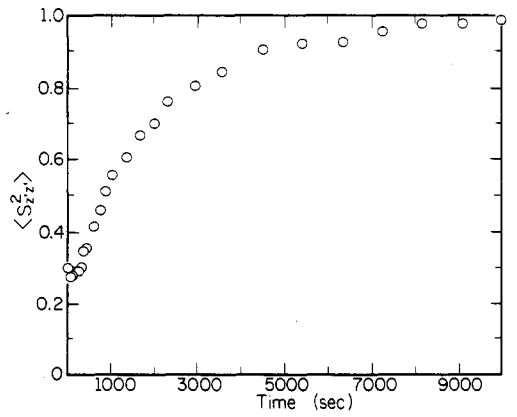

Figure 5. Plot showing the evolution of macroscopic orientation measured by $\langle S^2_{z'z'} \rangle$ as a function of time in the field.

ratio of the initial second moment to final second moment in a fully aligned specimen, $\langle \Delta\nu^2 \rangle^{i}_{M} / \langle \Delta\nu^2 \rangle^{0}_{M}$, should have, in principle, a value of 0.2 as well (see eq 6). We obtained an experimental value for this ratio which verifies our assumption that the asymptotic value of $\langle \Delta\nu^2 \rangle^{\circ}$ corresponds to that of a fully aligned sample with $\langle S^2_{z'z'} \rangle \approx 1.0$. Using data of the type shown in the graph of Figure 4, eq 10, and the proper values of $A_{\nu 0}/A_t$, $\langle \Delta\nu^2 \rangle^{\circ}$, and $\langle \Delta\nu^2 \rangle_I$, we can calculate $\langle S^2_{z'z'} \rangle$ as a function of time. A typical plot is shown in Figure 5, with an initial value of $\langle S^2_{z'z'} \rangle$ close to 0.2 as one would expect for random orientation.

In order to quantify orientation dynamics it is desirable to calculate a rate parameter from experimental data such as those shown in Figure 5. For this purpose one may consider the following model,[2] which describes orientation kinetics of a monodomain liquid crystal in a magnetic field. The process described by the model is that depicted on the top of Figure 1, involving the magnetic realignment of a monodomain of rodlike molecules. The driving force for magnetic alignment of liquid crystals is their anisotropic diamagnetic susceptibility and intermolecular cooperativity. In a magnetic field, the anisotropy gives rise to an orientation-dependent free energy given by

$$G = -\Delta\chi B^2(3 \cos^2 \theta_0 - 1)/6 \tag{11}$$

where $\Delta\chi$ is the difference between the parallel and perpendicular components of diamagnetic susceptibility, and B is the magnetic field strength. Since $\Delta\chi$ is positive for most thermotropic liquid crystals, free energy minimization is achieved at parallel alignment ($\theta_0 = 0°$). Although most molecules have anisotropic diamagnetic susceptibility, macroscopic orientation is not observed, given the absence of molecular cooperativity. This molecular cooperativity maintains the orientational order of liquid crystal phases disturbed by external forces. The physical result of cooperativity is a long-range magnetic torque in the mesophase. For small-molecule liquid crystals the orientational process has been described by an equation of motion expressed in terms of the magnetic torque, L_m, and the viscous torque, L_v. L_m tends to rotate the director into the field and is given by

$$L_m = -\tfrac{1}{2}(\Delta\chi)B^2 \sin 2\theta_0 \tag{12}$$

L_v, on the other hand, opposes this motion and can be expressed in terms of the rotational viscosity coefficient, γ_1, as

$$L_v = -\gamma_1(d\theta_0/dt) \tag{13}$$

Hence, the applicable equation of motion for the alignment of the mesophase director is

$$L_m + L_v = I(d^2\theta_0/dt^2) \tag{14}$$

where I is the moment of inertia. With the assumption of steady-state conditions, eq 14 simplifies to the form

$$2\tau(d\theta_0/dt) + \sin 2\theta_0 = 0 \tag{15}$$

where τ is a characteristic orientation time given by $\gamma_1/(\Delta\chi)B^2$. The solution to this equation

$$\tan \theta_0 = \tan \theta_0' \exp[-(t/\tau)] \tag{16}$$

describes the time dependence of the director orientation as it varies from some initial value of θ_0' to parallel alignment ($\theta_0 = 0°$). As it is written here, the equation assumes that the sample is a monodomain and can be described by a single orientation angle, θ_0.

Studies with small-molecule thermotropic LC's have shown that eq 16 adequately describes magnetic field reorientation of monodomains.[2] In these systems, τ values are reported to be on the order of 1 s at magnetic fields in the order of 1 T. Experimentally it is difficult to form monodomains of high molecular weight and high melting point thermotropic LCP's. Therefore, the experimental system required to verify the rate law shown above cannot be readily produced. The difficulty is the need to wait very long times at high temperature and/or the use of very high magnetic fields. However, the orientation rate law shown above has been applied to lyotropic and low molecular weight thermotropic LCP's. The few studies on polymeric systems have found less satisfactory agreement of the rate law in comparison to small-molecule liquid crystals. For example, magnetic susceptibility data studying the dynamics of alignment of the lyotropic LCP poly(benzyl L-glutamate) (PBLG) could not be completely fitted to the rate law over the entire time of observation (deviations were reported at short times).[11] Other work[15] has reported the reorientation time for a monodomain of a low molecular weight thermotropic polymer. Here it was concluded that the reorientation process could not be described by a single value of τ. The authors interpreted their results in terms of a distribution of rotational viscosities in nematic domains of varying molar mass.

As pointed out earlier, our studies have involved samples that initially have random molecular orientation. In our efforts to analyze experimental data, we have assumed that such samples might be physically described as having unoriented polydomain structure (see bottom of Figure 1). We emphasize, however, that such structural details of LCP mesophases remain unknown, and therefore our assumption is merely an iterative device to gain insight on structure vs. dynamics in these systems. Recall that from second-moment measurements we obtain the quantity

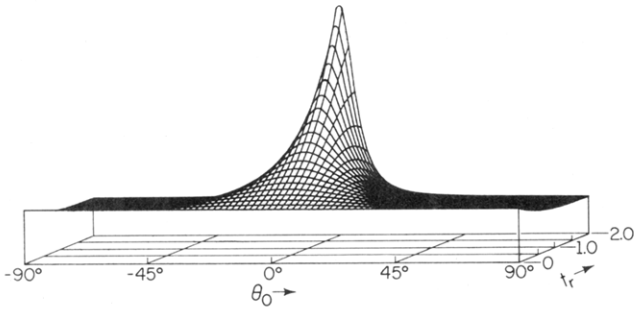

Figure 6. Orientational distribution of directors as a function of reduced time as predicted from the kinetic model. A random orientation of directors is assumed at $t_r = 0$.

$\langle S^2_{z'z'}\rangle$, which can reflect the orientational distribution of directors in our postulated polydomain sample. This time-dependent distribution can be represented mathematically as $\rho(\theta_0,t_r)$, where t_r is the reduced time variable t/τ. Since $S^2_{z'z'} = (^3/_2 \cos^2\theta_0 - {}^1/_2)^2$, the experimentally observed quantity $\langle S^2_{z'z'}\rangle$ can be calculated by averaging this function over the sphere of directions

$$\langle S^2_{z'z'}\rangle = \frac{\int_0^\pi \rho(\theta_0,t_r)[^3/_2 \cos^2\theta_0 - {}^1/_2]^2 \sin\theta_0\, d\theta_0}{\int_0^\pi \rho(\theta_0,t_r) \sin\theta_0\, d\theta_0} \quad (17)$$

The functional form of $\rho(\theta_0,t_r)$ is of course dependent on the choice of model used to describe the orientational process and on the initial orientational distribution in the sample. In our calculations we have used the rate model described earlier in this paper with initial conditions of random director orientation in the polydomain sample. In using this model we have furthermore assumed that domains orient independently of their neighboring domains. The distribution function that emerges from the model is given by

$$\rho(\theta_0,t_r) = \left[\frac{\sin[\tan^{-1}(\exp(t_r)\tan\theta_0)]}{\sin\theta_0}\right] \times \left[\frac{\exp(t_r)}{\cos^2\theta_0 + \exp(2t_r)\sin^2\theta_0}\right] \quad (18)$$

The Appendix describes selected steps in our derivation of this equation. In the limit of $t_r = 0$ this function takes on a value of unity at all angles and therefore satisfies the imposed initial condition. In the limit $t_r \to \infty$, on the other hand, $\rho(\theta_0,t_r)$ breaks down to a δ function having a value of infinity for $\theta_0 = 0°$ and a value of 0 at all other angles. Changes in this distribution function with increasing reduced times are shown in the plot of Figure 6. Substitution of eq 18 into eq 17 followed by integration over θ_0 allows us to calculate $\langle S^2_{z'z'}\rangle$ for a given value of t_r. The Appendix describes how this integration was carried out for analysis of data and it also describes an analytical solution of the integral that is applicable in the range of short reduced times. Repeating this procedure for various values of time and iteratively varying the parameter τ, we can generate the theoretical curve that gives the best fit to experimental data. The bottom curve in Figure 15 shows an example of a reasonable fit with a τ value of 32 s for a sample of intermediate molecular weight. The actual significance of this particular fit and that of others is discussed later in the paper.

Temperature Dependence. The dependence of alignment rate on temperature is revealed by plots in Figures 7 and 8. Figure 7 shows how $\langle S^2_{z'z'}\rangle$ changes with

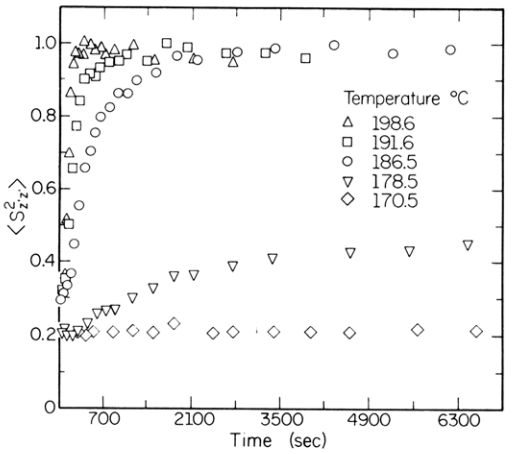

Figure 7. Kinetics of magnetic orientation at various temperatures for a sample with number-average molecular weight 6900.

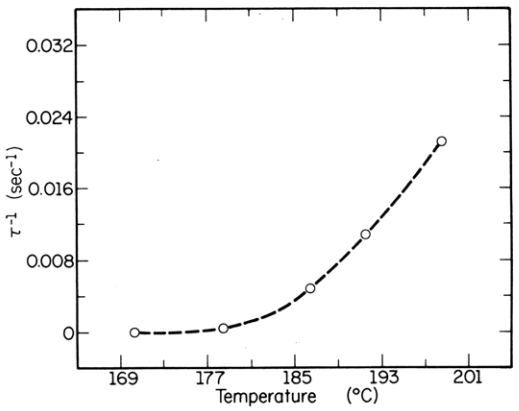

Figure 8. Rate constant for magnetic orientation plotted as a function of temperature.

Table I
Effect of Temperature on Characteristic Orientation Time

temp, °C	τ, s	temp, °C	τ, s
170.4	$>10^4$	191.6	92
178.5	2400	198.6	47
186.6	210		

time at various temperatures ranging from 170 to 200 °C. The number-average molecular weight of the sample used to generate these plots was 6900 as measured by vapor osmometry.[12] Table I lists the values of τ corresponding to the five different orientation temperatures used in the experiments. In Figure 8, the rate parameter τ^{-1} has been plotted as a function of temperature for this particular sample. Arrhenius behavior was not observed when the data were plotted as ln τ^{-1} vs. $1/T$. It is clear from data in Figures 7 and 8 that no significant macroscopic orientation occurs on the time scale of our experiments at temperatures below 170 °C even though the most prominent endothermic transition in the DSC spectrum occurs around 145 °C.[12] We do not know at this point what structural changes are association with this particular k′ → LC transition. We refer to the solid phase as k′ rather than k in recognition of its undefined structural nature.

We have characterized our material by high-resolution NMR as being chemically disordered;[12] however, some diffraction is observed in X-ray photographs of solid samples. It is for this reason that we refer to the material's solid structure as not being classically defined. Through our own optical microscopy studies[12] we have characterized our polymer as a nematic LC above 185 °C. However, we do not know if the DSC main endotherm represents a k′

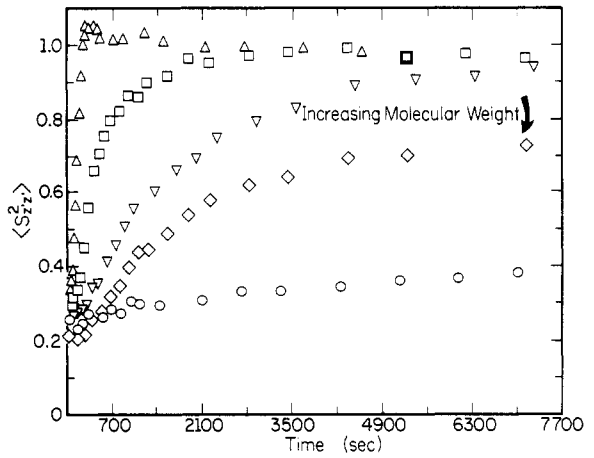

Figure 9. Kinetics of magnetic orientation at T = 185 °C for samples varying in molecular weight.

→ N transition or if a more ordered and/or more cohesive mesophase precedes the nematic state. The low-temperature mesophase (below 185 °C) could be a smectic LC, a biaxial nematic, or a nonclassical nematic that contains localized smectic regions or crystallites. Close inspection of the DSC scan[12] reveals the possibility of a second broad endotherm in the range 155–170 °C. It is even possible that the more ordered mesophase forms as a result of "recrystallization" (resolidification) during the DSC scan. In any event, the presence of a more ordered and/or cohesive mesophase following the DSC main endotherm could explain the observed drastic change in orientation rate as temperature is increased from 176.5 to 186.5 °C. This drastic change in alignment kinetics with a 10 °C change in temperature is clearly revealed by Figures 7 and 8.

Molecular Weight Dependence. We investigated the effect of molecular weight on the kinetics of magnetic alignment. Data on $\langle S^2_{z'z'}\rangle$ as a function of time for various molecular weights are shown in Figure 9. As indicated in this figure, there is a very significant difference in alignment kinetics among the five different molecular weights used in the experiments. This is especially true if one compares data for samples having the highest and lowest molecular weight. The lowest molecular weight samples align almost instantly to a value of $\langle S^2_{z'z'}\rangle$ of approximately 1.0 (full alignment). In contrast, the highest molecular weight sample remains essentially in random orientation after a time period of approximately 5 h. However, an extremely slow climb to a more aligned state can be observed in these high molecular weight samples. Interestingly, the molecular weight range between the two extremes involves approximately only a factor of 4 (3900 vs. 15 800). This observation suggests a great sensitivity of orientation rate on molar mass in spite of liquid crystal order.

We attempted to fit the theoretical curve described above to orientation kinetics data for samples with different molecular weights. Figure 10 shows the typical results obtained after fitting theoretical curves by adjustment of the parameter τ. We observe the most reasonable fit of experimental data to the model in samples of low molecular weight (see Figure 10). As exemplified by the top curve in Figure 10, it is possible that positive deviations from theory are observed with the best possible fit in low molecular weight samples. By positive deviation we mean that the observed orientation rate is faster than predicted by the fitted curve derived from the model. In contrast, as molecular weight increases, the experimental curves exhibit progressively larger negative deviations from

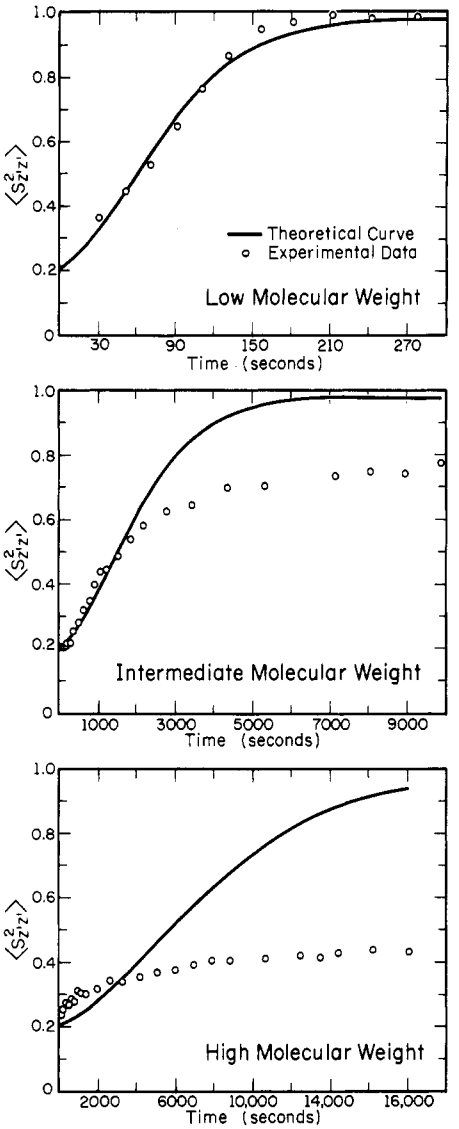

Figure 10. Comparison of the experimentally measured time dependence of macroscopic order, $\langle S^2_{z'z'}\rangle$, to that predicted by the kinetic model (solid line) as a function of time for samples with low, intermediate, and high molecular weight. Note the abscissa scale is different in the three plots.

theory at long times (Figure 10). Recall that the theoretical model used assumes that samples behave as though they were composed of domains that are randomly oriented prior to magnetic exposure. Most importantly, this model also assumes that such domains reorient independently. We have not expected a priori that such a simple model for the realignment process would be adequate for such complex systems as polymeric mesophases. However, observing the negative and perhaps positive deviations from the model at high and low molecular weights, respectively, can be helpful in gaining some insight on the structure of LCP's. We infer that any positive deviations at low molecular weight could imply interdomain cooperativity during the reorientation process. Such cooperativity would originate in the participation of a single chain in various LC domains. One might expect that the full impact of domain interdependence is sensed when the macroscopic order parameter has increased significantly. This would then be consistent with the possible positive deviation in the region of high macroscopic order parameter.

If chains traverse more than one domain, one has to consider the existence of at least short segments, which

Table II
Effect of Molecular Weight on Characteristic Orientation Time

mol wt	τ_N,[a] s	τ_A,[b] s	γ_1, P
3900	46	38	1.0×10^4
6900	210	122	4.6×10^4
8700	775	417	1.7×10^5
14800	1300	804	2.9×10^5
15800	4500	4170	9.9×10^5

[a] Calculated by numerical integration of eq 17. [b] Calculated by approximate analytical form of eq 17.

might be viewed as defects in the uniaxial LC phase. When the molecular weight is low, such defects may not interfere severely with macroscopic alignment of the mesophase. On the other hand, negative deviations at high molecular weight could imply that a larger fraction of chain segments are found in these defective interdomain regions. On the basis of our data, one could infer that such regions are more abundant in high molecular weight samples. Furthermore, chain segments that reside within such boundary zones may possess very low order and would be therefore unable to contribute to cooperative alignment. Further evidence for these possibilities is discussed later in this section. In the context of our observed slow reorientation in high molecular weight samples, the presumed boundary contributes significantly to the viscous torque opposing macroscopic alignment. One may also expect that this opposition depends in some way on the molecular flexibility of segments within the boundary. If one considers the positive and negative deviations in the molecular weight extremes, it is not surprising that reasonable fits to the model are obtained at low molecular weights. One may simply state that the simultaneous contributions of domain cooperativity and boundary zone viscosity could fortuitously produce a reasonable fit to experimental data. Therefore, we emphasize that the fact that we can obtain reasonable fits in some cases does not imply that the model is a good physical description of the mesophase and its dynamics.

Viewing the model as a tool to quantify orientation rate, we thought it would be instructive to examine the molecular weight dependence of τ. Since all samples yield a reasonable fit within the range of short reduced times, we proceeded to calculate an initial τ value as a function of molecular weight. Table II lists values of τ calculated by two different methods described earlier (numerical integration and the approximate analytical solution). The τ values of this table correspond to samples with various molecular weights. Figure 11 shows plots of τ^{-1} vs. intrinsic solution viscosity and its corresponding log–log plot. The estimated values of molecular weight corresponding to these viscosities are given in the previous paper of this series.[12] Following our orientational model, we expect the τ^{-1} parameter to vary inversely with rotational viscosity (γ_1). On the basis of the physics of nematic polymers, such friction coefficients are expected to scale like M^2, where M is the molecular weight.[16] In principle, this result is applicable to nonentangled melts of rodlike chains. However, as pointed out by de Gennes,[16] when entanglements are dominant, conventional reptation arguments predict that such friction coefficients scale as M^3. One may therefore expect that τ^{-1} should scale as some power of M which reflects chain topology in the LC state. Using samples that have been aged to 200 °C for 1 h prior to magnetic alignment, we find that

$$\tau^{-1} \sim M^{-n} \tag{19}$$

where $n \geq 3.1$. If we combine vapor osmometry data of molecular weight with intrinsic viscosity measurements and calculate this way a value for the Mark–Houwink constant α, then $n = 3.1$. On the basis of data discussed later in the paper, we expect n to depend sensitively on isothermal aging history. That is, values of n above and below 3.1 could be measured, depending on aging. It is interesting that the dependence of the rate parameter on molecular weight can resemble that expected from flexible and entangled macromolecules. Whether or not this means that more flexible and entangled chain segments exist in what might be an interphase region is a concept that we cannot precisely determine from our data. However, it is possible that if such flexible chain segments exist in a boundary zone between domains, they could raise significantly the viscous resistance to magnetic orientation.

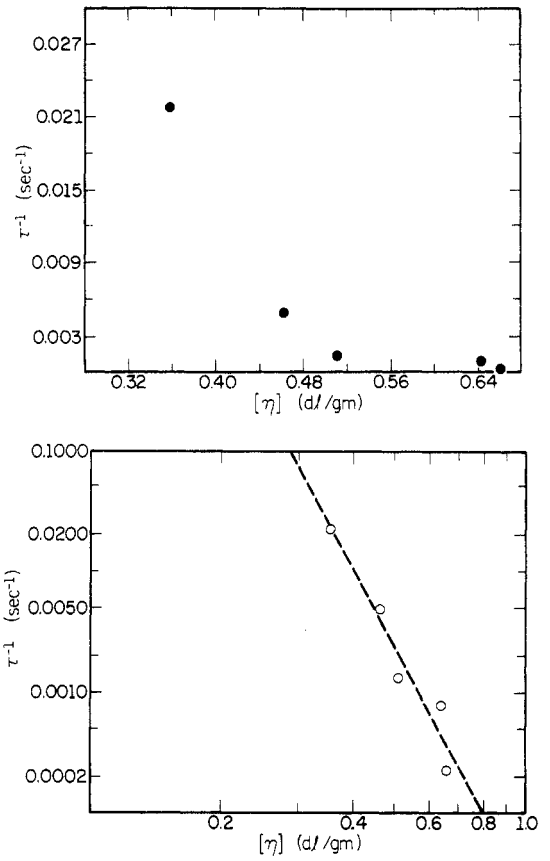

Figure 11. Rate constant for magnetic orientation of pure melt as a function of dilute solution intrinsic viscosity of the corresponding polymer (top). Same data shown as a log–log plot (bottom).

The magnitude of the rotational viscosity coefficient can be estimated from experimental τ values, and this may provide further information about the microstructure of the polymeric mesophase. Hardouin et al.[4] have measured $\Delta\chi$ for polyesters chemically identical with those studied here and found a value of 1.0×10^{-7} emu cgs g^{-1}. Thus, the rotational viscosity coefficient can be calculated from the expression

$$\gamma_1 = \tau B^2 \Delta\chi \tag{20}$$

Within the range of molecular weights studied in our work, γ_1 values were found to vary between 1×10^4 and 9×10^5 P for the lowest and highest molecular weight samples, respectively (see Table II). Interestingly, these calculated magnitudes of γ_1 are on the same order of magnitude as those corresponding to non-liquid crystalline condensation polymers. Recently, Zheng-Min and Kleman[17] measured the rotational viscosity coefficient for LC polyesters in

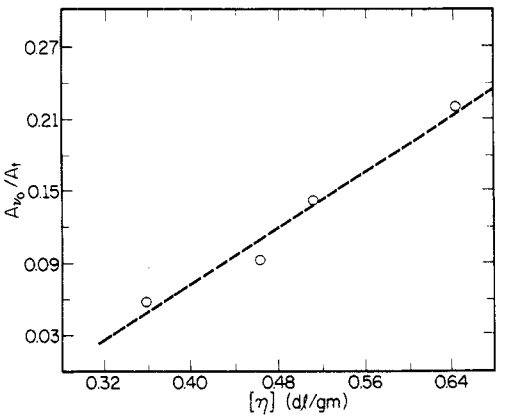

Figure 12. Fraction of area under the central resonance peak of liquid crystal melts ($A_{\nu 0}/A_t$) plotted against dilute solution intrinsic viscosity of the corresponding polymers.

well-oriented monodomain specimens. They report γ_1 values on the order of 1×10^2 P for the same polyester used in our investigation. The large difference between those values and ours (1–3 orders of magnitude higher in our case) may reflect some fundamental differences in the dynamics of polydomain vs. monodomain polymeric mesophases. The large magnitude of γ_1 is consistent with the notion that less-ordered chain segments in an interphase region create a significant viscous resistance to domain alignment.

The next logical question to ask is what evidence is there for the existence of an interphase. Referring back to Figure 3, we note the coexistence of a central resonance peak in the NMR spectrum even when complete macroscopic alignment is achieved. Previous investigators have offered explanations for the presence of this central peak. Recently Brückner et al.[14] attributed the peak to the presence of an isotropic phase that coexists with the liquid crystal phase. Other investigators have made similar proposals.[18] In attempting to interpret the origin of the central peak, one should consider the work of Schmiedel et al.[19] These authors have shown in calculated NMR spectra for small-molecule liquid crystals that the central peak appears in fully aligned samples when certain levels of intramolecular motion are allowed in the mesogen. In this context, one could have assumed that intramolecular mobility in the spacer of our polymer is sufficient to generate the central peak. However, the work of Brückner et al.[14] shows that this central peak is observed by proton NMR even when the spacer is fully deuteriated. In other work, the central peak has been resolved and shown to contain contributions from both aliphatic and aromatic components.[18] These experimental results therefore suggest a possible link between the central peak and the presence of a more mobile (inter)phase. The presence of an interphase or several phases that differ in their molecular mobility at a given temperature could be accounted for in several ways. These regions could not only differ in being isotropic vs. liquid crystalline but other more subtle differences between them might be considered as well. Two examples would be a biaxial nematic phase vs. a uniaxial nematic phase, and less likely, yet possible, smectic vs. nematic character. What seems apparent from previous work is that the central resonance peak can be associated with a fraction of more mobile chains or chain segments within these materials. Other issues such as the size of the mobile and less mobile regions as well as the sharpness of boundaries between these regions are currently unknown.

We examined the dependence of the area under the central peak, $A_{\nu 0}$, on molecular weight. Figure 12 shows a plot of fractional area under the central peak, $A_{\nu 0}/A_t$, in aligned mesophases vs. intrinsic solution viscosity of the corresponding polymer. It is apparent from these data that samples with higher molecular weight have a greater fraction of the more mobile segments. This fraction ranges from 0.06 to 0.21 for chains having molecular weights between 3900 and 14 800, respectively. On the basis of these data and the well-known fact that microscopic order increases with molecular weight,[20] it is difficult to attribute the central peak to mobile segments in a single, homogeneous liquid crystalline phase. If it were a single phase, one would predict a decreasing level of molecular mobility within LC domains with an increase in both molecular weight and microscopic order parameter. Thus, the trend we find for $A_{\nu 0}/A_t$ vs. $[\eta]$ is consistent with the idea of a multiphasic structure or one with interphases composed of regions having different motional characteristics. Since the fraction of the more mobile phase seems to increase with molecular weight, it is also difficult to attribute its presence to low molecular weight material. The central peak is essentially absent in the lowest molecular weight samples synthesized in our laboratory (these particular samples were not included in our alignment rate studies since their kinetics are impractically fast). Therefore, on the basis of our data, an interphase with greater molecular mobility can be visualized as composed of traversing "chain segments" with less orientational or positional order than those in the more ordered region(s). One of the physical pictures that would be consistent with our results is that of the mesophase with the structure of a "liquid fringed micelle".

Alternatively, rather than invoking traversing chain segments, one could propose a more mobile phase(s) composed of segregated chains of either high molecular flexibility or low molar mass. In order for the idea of segregated low molar mass material to be consistent with our data, one has to postulate a significant increase in polydispersity with molecular weight. Using a chemical model of our polymerization and a computational method described by Lopez-Serrano et al.,[21] we performed calculations of polydispersity as a function of extent of reaction.[12] The results indicate that within the extent of reaction values involved in our molecular weight range, the predicted differences in polydispersity are negligible (1.85 vs. 1.98 from our lowest to our highest molecular weight). On the basis of these results and other experimental evidence that we discuss below, it is difficult for us to link the apparently more mobile regions to segregated low molar mass material. As mentioned above, the other possibility one could consider is the segregation of chains or chain segments on the basis of molecular flexibility. If one postulates a molecular "flexibility distribution", related or unrelated to molecular weight distribution, this type of segregation is conceivable. However, other data presented below make it difficult to associate the mobile component in these particular samples with phase-separated high-flexibility "chains" as opposed to chain segments. As it will be apparent from the following discussion, segregation of more flexible "chain segments" is still a plausible interpretation. So far our data suggest that the fraction of more mobile segments within some boundary zone or additional phase(s) increases with higher degree of polymerization. As we have already suggested, such a boundary zone could strongly retard the kinetics of magnetic orientation, depending on the molecular rigidity of its segments. Thus, the concept of increasing fractions of chain segments within a boundary zone or interphase at increasing degrees of polymerization would be consistent with our kinetic

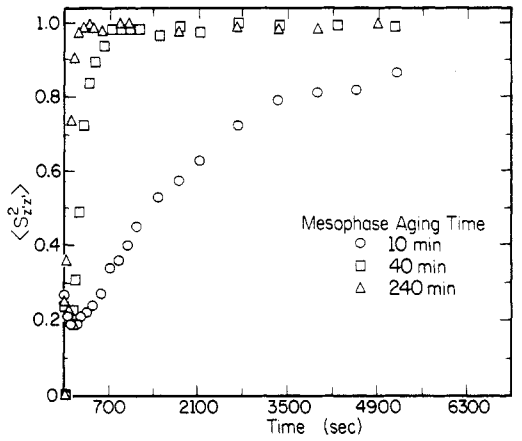

Figure 13. Kinetics of magnetic orientation of samples isothermally aged in the mesomorphic state for various lengths of time. The molar mass of these samples was 8700 and the data were recorded at 185 °C.

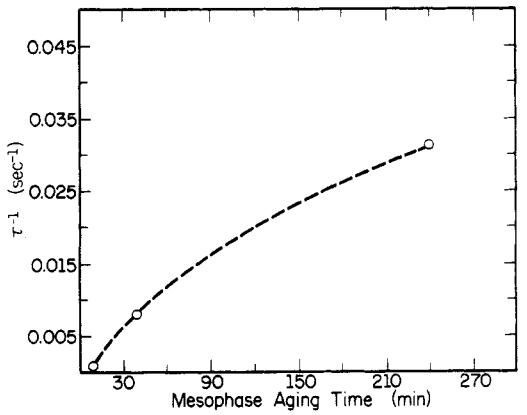

Figure 14. Plot of magnetic orientation rate constant as a function of mesophase aging time at 200 °C. The molecular weight of the sample was 8700 and the data were recorded at 185 °C.

Table III
Effect of Mesophase Aging on Characteristic Orientation Time

aging time, min	τ, s
10	1260
40	125
240	32

measurements. A question not discussed so far is the thermodynamic vs. kinetic origin of the apparent interphase or multiphasic structure. Some experiments related to this issue are described below.

Mesophase Aging Effect. On the basis of earlier work in our laboratory involving surface orientation of LCP's,[22] we were aware of the fact that thermal history of the mesophase played an important role on backbone alignment. Extending this concept to kinetics of magnetic alignment, we discovered very interesting phenomena. For example, the orientation rate constant τ^{-1} can be increased by more than 1 order of magnitude simply by isothermal aging of the sample at temperatures above the solid to liquid crystal transition (see Table III). Figures 13 and 14 show how alignment kinetics and corresponding rate constants vary with mesophase aging time at a temperature of 200 °C. It is apparent from these data that aging of the mesophase causes a dramatic increase in τ^{-1}. It is interesting to note in Figure 15 that significantly better fits of experimental data to theoretical curves are obtained in isothermally aged samples. In the context of earlier discussion, this result suggests greater orientational independence for domains with thermal aging. The specific implication of the data is a gradual decrease of viscous resistance to orientation with further aging.

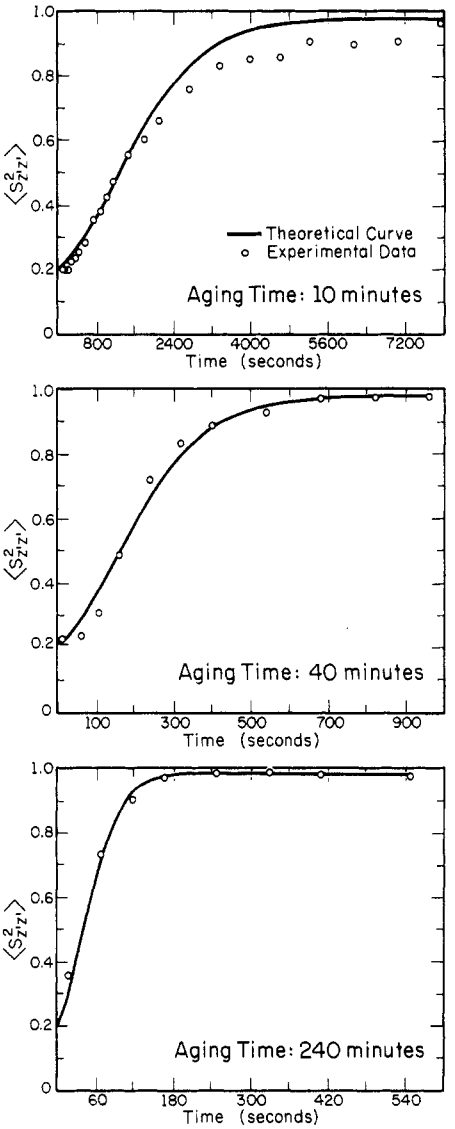

Figure 15. Comparison of the experimentally measured time dependence of macroscopic order parameter, $\langle S^2_{z'z'}\rangle$, to that predicted by the kinetic model in samples aged for various times. Note the abscissa scale is different in the three plots. The molar mass of these samples was 8700 and the data were recorded at 185 °C.

Table IV
Effects of Mesophase Aging on Chain Microstructure

	structural unit composition			oxybenzoate sequence length	
sample	pimeloate	oxybenzoate	dioxyphenyl	exptl	calcd[a]
pristine material	0.38	0.24	0.38	1.34	1.32
mesophase aged material[b]	0.37	0.26	0.37	1.33	1.35

[a] A random microstructure was assumed. [b] 200 °C, 1 h.

Since polyesters similar to the one we studied are known to undergo transesterification reactions, we characterized first the effect of aging on chain microstructure. For this purpose, high-resolution ^{13}C NMR spectroscopy can provide useful information. In Table IV we have summarized structural unit composition and oxybenzoate sequence length ($\bar{l}_{OB}$) data for a specimen prior to and after mesophase aging. Also shown in Table IV is the oxybenzoate

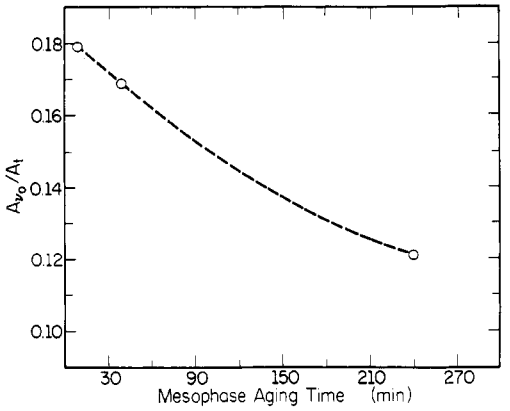

Figure 16. Fraction of area under the central resonance peak ($A_{\nu 0}/A_t$) plotted as a function of mesophase aging time. The molar mass of these samples was 8700 and the data were recorded at 185 °C.

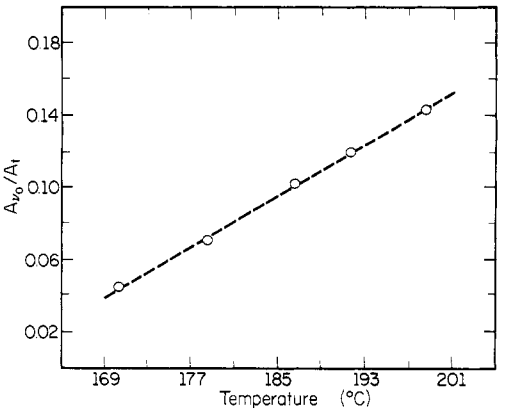

Figure 17. Fraction of area under the central resonance peak ($A_{\nu 0}/A_t$) as a function of temperature for a sample with a molar mass of 6900.

sequence length calculated for a random microstructure with the proper structural unit compositions. It is clear from these results that within experimental error both samples possess essentially random microstructures at the diad level before and after the aging treatment. Also, we were unable to detect significant changes in intrinsic viscosities of the polymer after aging periods. The largest decrease we detected amounted to less than 5% for samples aged 250 min (the experimental resolution was approximately 3%). On the basis of all our kinetic data, if molecular weight changes were the dominant mechanism in aging, we would expect a reduction in intrinsic viscosity in the order of 20% after this prolonged aging time. In view of these findings, we believe that changes in chemical microstructure do not contribute significantly, if at all, to the observed dependence of orientation rate on isothermal aging of the mesophase.

In an attempt to understand the physical basis of the mesophase aging effect, we measured the dependence of $A_{\nu 0}/A_t$ on aging time. The results revealed a significant decrease in $A_{\nu 0}/A_t$ with increasing aging time (see Figure 16). Given this result, it is once more a problem to associate the central peak with segregated low molecular weight material. The difficulty lies in understanding why the initial segregation by molar mass would reverse with isothermal aging. As we have described above, $A_{\nu 0}/A_t$ can be interpreted as a measure of the fraction of chain segments in a boundary zone separating what might be more ordered LC domains. Viewed in this context, data shown in Figure 16 suggest that the fraction of segments in the more mobile boundary zone decreases with time. In other words, the suggestion is that chain segments in the less ordered boundary region become incorporated with time in the more ordered domain environment. The consequent growth of the more ordered phase allows the system to align more cooperatively in the magnetic field. This is consistent with our earlier suggestion that chain segments in the boundary zone can be a rate-limiting element in orientation dynamics, and therefore it follows that aging leads to significantly faster alignment kinetics. We observed the effect in both "as-synthesized" polymer and polymer that was "solution precipitated" in a nonsolvent after the original synthesis. Depending on the fraction of mobile segments, other segregation mechanisms could occur that do not involve the growth of the ordered regions. In order to explore this possibility one clearly needs other systems. This is an area we plan to explore in future work.

The implication of the aging effect is that the apparent interphase or multiphasic structure is not at thermodynamic equilibrium. The equilibrium structure may contain an interphase or several phases. Another possibility is that the equilibrium structure is closer to that of a single phase with the inevitable defects of liquid crystals and those of chemically inhomogeneous polymers. It is clear that this issue remains unresolved and will need to be addressed in future experiments and theories of liquid crystallinity in polymers. Finally, we point out our observation that central peak area increases with temperature (Figure 17). This increase could result from greater levels of rotational motion in both phases. Therefore, it is difficult to infer very much on the nature of structure from the temperature dependence of the central peak.

Our data on orientation kinetics suggest a great deal of interdependence among the various regions in the fluid state. On this basis, one must consider the possibility of long-range correlations over distances greater than the size scale of ordered domains and their boundary regions. Therefore, supermolecular entities may also exist in the fluid as a consequence of interdomain connectivity. Finally, we point out that solidification of the fluid mesophase could result in a significant rearrangement of the structure. It would therefore be wrong to assume that the solid-state structure is merely the vitrification of the fluid microstructure. For example, when solidification occurs, chain segments in the less ordered regions may be incorporated in the more ordered phase, thus leading to poorer interconnection between solid lamellae. These topics are clearly very important in a materials science context and must be studied in great detail.

Conclusions

This work has studied the orientation kinetics of a main-chain liquid crystal polymer in a magnetic field. Several aspects of the molecular microstructure associated with the fluid mesophase can be inferred from the experimental results. We conclude that an interphase or multiphasic structure exists and that a single chain can traverse several of these regions. The fluid microstructure suggested by the data is reminiscent of the solid semicrystalline morphology of flexible macromolecules. We believe the regions differ in the nature of order and motional characteristics of their chain segments. Our data indicate that the interphase or multiphasic structure is not at equilibrium in the as-synthesized polymer. The tendency in the specific samples studies is for the more ordered regions to gradually incorporate segments that reside in less ordered regions. One of the interesting properties suggested by the data is the rate-limiting role in orientation kinetics of the less ordered component present only in small mole fractions ranging from 0.06 to 0.21. This minor

component might be responsible for the observed scaling behavior of a rotational viscosity coefficient, $\gamma_1 \sim M^n$, where M is molecular weight and $n \geq 3.1$. On the basis of our data, an important future direction is to understand the thermodynamics and possible means for external or synthetic control of the less ordered regions. Such efforts will be required in order to take full advantage of liquid crystal properties in polymers.

Appendix

A small solid angle is denoted $d\Omega$, where

$$d\Omega = 2\pi \sin \theta_0 \, d\theta_0 \tag{1A}$$

Let n be equal to the total number of domains in a spherical unit volume and dn be equal to the number of domains within a cone of solid angle $d\Omega$ at time t_r

$$dn = \rho(\theta_0,t_r) \, d\Omega \tag{2A}$$

One may write

$$\rho(\theta_0,t_r) = \frac{dn}{d\Omega'} \frac{d\Omega'}{d\Omega} \tag{3A}$$

where $d\Omega'$ is equal to the cone of solid angle in which domains reside at $t_r = 0$. If one assumes random orientation at $t_r = 0$, then the initial distribution, $dn/d\Omega'$ is a constant. Assuming for convenience that $dn/d\Omega' = 1$

$$\rho(\theta_0,t_r) = \frac{d\Omega'}{d\Omega} = \frac{\sin \theta_0' \, d\theta_0'}{\sin \theta_0 \, d\theta_0} \tag{4A}$$

On the basis of the model used in the text, a given domain making an angle θ_0' at $t_r = 0$ will make an angle θ_0 at some finite t_r

$$\tan \theta_0 = \tan \theta_0' \exp(-t_r) \tag{5A}$$

Solving (5A) for θ_0' as a function of θ_0 gives

$$\theta_0' = \tan^{-1} [\exp(t_r) \tan \theta_0] \tag{6A}$$

The derivatrive of (6A) with respect to θ_0 is

$$\frac{d\theta_0'}{d\theta_0} = \frac{\exp(t_r)}{\cos^2 \theta_0 + \exp(2t_r) \sin^2 \theta_0} \tag{7A}$$

From eq 6A, 7A, and 4A, it follows that

$$\rho(\theta_0,t_r) = \left[\frac{\sin [\tan^{-1} (\exp(t_r) \tan \theta_0)]}{\sin \theta_0} \right] \times \left[\frac{\exp(t_r)}{\cos^2 \theta_0 + \exp(2t_r) \sin^2 \theta_0} \right] \tag{8A}$$

The integral in eq 17 was solved numerically to fit data to the theoretical model. The method used for this integration was the 1/3 Simpson rule, and the range was divided into 180 intervals. In the limit of short reduced times, $\sin \theta_0'/\sin \theta_0 \approx 1$, and eq 8A simplifies to

$$\rho(\theta_0,t_r) = \frac{\exp(t_r)}{\cos^2 \theta_0 + \exp(2t_r) \sin^2 \theta_0} \tag{9A}$$

Using eq 9A, we solved analytically the integral in eq 17, and data in Table II show values of τ calculated with this approximation and with the numerical integration. As suggested by the table, agreement between the analytical approximation and the numerical integration is observed for low molecular weight samples. The analytical solution involved the following expansion:

$$\frac{k}{4I} \int_0^\pi \frac{(3 \cos^2 \theta_0 - 1)^2 \sin \theta_0}{\cos^2 \theta_0 + k^2 \sin^2 \theta_0} \, d\theta_0 = \frac{k}{4I} \int_0^\pi \left[\frac{9 \cos^4 \theta_0 \sin \theta_0}{\cos^2 \theta_0 + k^2 \sin^2 \theta_0} - \frac{6 \cos^2 \theta_0 \sin \theta_0}{\cos^2 \theta_0 + k^2 \sin^2 \theta_0} + \frac{\sin \theta_0}{\cos^2 \theta_0 + k^2 \sin^2 \theta_0} \right] d\theta_0 \tag{10A}$$

where

$$k = \exp(t_r)$$

$$I = \int_0^\pi \rho(\theta_0,t_r) \sin \theta_0 \, d\theta_0$$

This expression is followed by the substitution

$$z = \tan (\theta_0/2)$$

After this substitution we carried out a partial fraction decomposition of all integrals in the expansion. We show below the simplest example of this decomposition

$$\frac{\sin \theta_0}{\cos^2 \theta_0 + k^2 \sin \theta_0} = \frac{z}{(1 + \beta_+ z^2)(1 + \beta_- z^2)} \tag{11A}$$

where

$$\beta_+ = \tfrac{1}{2}[-K + (K^2 - 4)^{1/2}]$$

$$\beta_- = \tfrac{1}{2}[-K - (K^2 - 4)^{1/2}]$$

$$K = 4k^2 - 2$$

Partial fraction decomposition and integration yield

$$\frac{\sin \theta_0}{\cos^2 \theta_0 + k^2 \sin \theta_0} = 2k \left[\frac{1}{(K^2 - 4)^{1/2}} \ln \left[\frac{K + (K^2 - 4)^{1/2}}{K - (K^2 - 4)^{1/2}} \right] \right]$$

The other integrals were handled similarly but their decompositions involved solving up to six simultaneous equations.

References and Notes

(1) Carr, E. F. *Mol. Cryst. Liq. Cryst.* **1969**, *7*, 253.
(2) Wise, R. A.; Olah, A.; Doane, J. W. *J. Phys. (Les Ulis, Fr.)* **1975**, *36*, 117.
(3) Martins, A. F.; Ferreira, J. B.; Volino, F.; Blumstein, A.; Blumstein, R. B. *Macromolecules* **1983**, *16*, 279.
(4) Hardouin, F.; Achard, M. F.; Gasparoux, H.; Liebert, L.; Strzelecki, L. *J. Polym. Sci., Polym. Phys. Ed.* **1982**, *20*, 975.
(5) Maret, G.; Blumstein, A. *Mol. Cryst. Liq. Cryst.* **1982**, *88*, 295.
(6) Liebert, L.; Strzelecki, L.; van Luyen, D.; Levelut, A. M. *Eur. Polym. J.* **1981**, *17*, 71.
(7) Noel, C.; Monnerie, L.; Achard, M. F.; Hardouin, F.; Sigaud, G.; Gasparoux, H. *Polymer* **1981**, *22*, 578.
(8) Sigaud, G.; Yoon, D. Y.; Griffin, A. C. *Macromolecules* **1983**, *16*, 875.
(9) Platonov, V. A.; Litovchenko, G. D.; Belousova, T. A.; Mil'kova, L. P.; Shablygin, M. V.; Kuhlichikhin, V. G.; Papkov, S. P. *Polym. Sci. USSR (Engl. Trans.)* **1976**, *18*, 256.
(10) Panar, M.; Beste, L. F. *Macromolecules* **1977**, *10*, 1401.
(11) Sridhar, C. G.; Hines, W. A.; Samulski, E. T. *J. Chem. Phys.* **1974**, *61*, 947.
(12) Moore, J. S.; Stupp, S. I. *Macromolecules*, preceding paper in this issue.
(13) Doane, J. W. In *Magnetic Resonance of Phase Transitions*; Owens, F. J., Poole, C. P., Jr. Farach, H. A., Eds.; Academic: New York, 1979; p 171.
(14) Brückner, S.; Scott, J. C.; Yoon, D. Y.; Griffin, A. C. *Macromolecules* **1985**, *18*, 2709.
(15) Volino, F.; Allonneau, J. M.; Giroud-Godquin, A. M.; Blumstein, R. B.; Stickles, E. M.; Blumstein, A. *Mol. Cryst. Liq. Cryst. Lett.* **1984**, *102*, 21.

(16) de Gennes, P.-G. In *Polymer Liquid Crystals*; Ciferri, A., Krigbaum, W. B., Meyer, R. B., Eds.; Academic: New York, 1982; p 115.
(17) Zheng-Min, S.; Kleman, M. *Mol. Cryst. Liq. Cryst.* **1984**, *111*, 321.
(18) Nicely, V. A., unpublished data.
(19) Schmiedel, H.; Hillner, B.; Grande, S.; Losche, A.; Limmer, S. *J. Magn. Reson.* **1980**, *40*, 369.
(20) Blumstein, A.; Asrar, J.; Blumstein, R. B. In *Liquid Crystals and Ordered Fluids*; Griffin, A. C., Johnson, J. F., Eds.; Plenum: New York, 1984; Vol. 4, p 311.
(21) Lopez-Serrano, F.; Castro, J. M.; Macosko, C. W.; Tirrell, M. *Polymer* **1980**, *21*, 263.
(22) Martin, P. G.; Stupp, S. I. "Solidification of a Main-Chain Liquid Crystalline Polymer: Effects of Electric Fields, Surfaces, and Mesophase Aging" submitted for publication.

Possible Chain Conformations in the Crystalline State of a Series of Mesogenic Polymers

Finizia Auriemma, Paolo Corradini,* and Angela Tuzi

Dipartimento di Chimica, Università di Napoli, Via Mezzocannone 4, Napoli, Italy.
Received April 2, 1986

ABSTRACT: The chain repetition periods in the crystalline state for the series of polymers [–1,4-$C_6H_4C(CH_3)$=N—N=$C(CH_3)$-1,4-$C_6H_4OOC(CH_2)_{n-2}COO$–]$_x$ with n = 8, 9, ..., 13 were determined. Through an analysis of the possible chain symmetries satisfying the equivalence principle and on the basis of simple energetic considerations, chain models of these polymers reproducing the experimental periods are outlined. The resulting conformations are such that the elongation axis of the rigid groups –1,4-$C_6H_4C(CH_3)$=N—N=$C(CH_3)$-1,4-C_6H_4– is significantly displaced from alignment with the chain axis. A proposal for the quantitative evaluation of the chain "waviness" of the polymers studied is presented.

Introduction

As has been shown in preceding papers,[1–3] mesophasic polymers can be obtained if rigid groups like –1,4-$C_6H_4C(CH_3)$=CH-1,4-C_6H_4– or –1,4-$C_6H_4C(CH_3)$=N—N=$C(CH_3)$-1,4-C_6H_4– are introduced with regularity within a flexible chain.

Thermodynamic studies have been performed on such polymers,[4,5] but only preliminary structural studies have been performed until now. In particular, the solid-state polymorphism of poly[oxydodecanedioyloxy-1,4-phenylene(2-methylvinylene)-1,4-phenylene] was investigated[6] and the structures of some low molecular weight model compounds were solved,[7,8] with the aim of obtaining indications useful for the establishment of the chain conformation in the crystalline state of homologous polymeric compounds. In this paper we are interested in studying the chain conformation in the crystalline state of polymers of the kind [–1,4-$C_6H_4C(CH_3)$=N—N=$C(CH_3)$-1,4-$C_6H_4OOC(CH_2)_{n-2}COO$–]$_x$ with n = 8–13. The thermal behavior of the polymers has already been characterized;[4] they show nematic mesophases with strong odd–even effects.

In this paper we shall discuss the possible chain conformations that are compatible with the experimental chain repetition periods for the polymers of the series having both an odd number and an even number of carbon atoms in the aliphatic chain and that satisfy the minimum energy and equivalence principle.[9]

Experimental Section

The series of polymers considered, [–1,4-$C_6H_4C(CH_3)$=N—N=$C(CH_3)$-1,4-$C_6H_4OOC(CH_2)_{n-2}COO$–]$_x$, comprises chains with n = 8–13. Hereafter, we shall indicate such polymers with the notation P_n, with n varying in the range indicated. The preparation of the polymers has been carried out according to a method already described.[1]

Fibers suitable for X-ray analysis were hot extruded.

Table I shows the chain identity periods (c) experimentally determined from fiber and tilted fiber spectra. The X-ray films showed good crystallinity but poor orientation so that the experimental periods are affected by the rather large errors indicated.

Scheme I

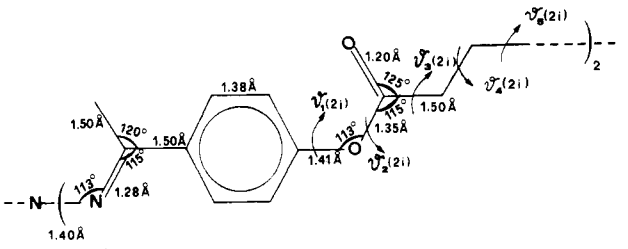

Table I
Experimental Identity Periods for the Polymers under Study

polymer	c/Å	polymer	c/Å
P_8	23.3 ± 0.8	P_{11}	46.7 ± 1.1
P_9	41.9 ± 1.3	P_{12}	28.4 ± 1.3
P_{10}	26.1 ± 0.7	P_{13}	53.4 ± 1.0

Geometrical and Energetic Considerations

The internal coordinates for the chain conformation of all the models studied have been chosen in conformity with the following geometrical and energetic considerations.

Bond Lengths and Valence Angles. Standard values of 1.54 Å and 112° have been used for the carbon atoms of the aliphatic chain. Values for the ester group have been chosen according to the results of structural studies on low molecular weight compounds[7,8] and according to literature data.[10] Values for the rigid group have been chosen according to ref 7 and 11.

Scheme I shows, in parentheses, half of the ith constitutional repeating unit, together with the values used for bond lengths and valence angles and the notation used for the torsion angles.

Torsion Angles. The rigid group has been assumed to be planar;[7] the torsion angles ϑ_2 (see Scheme I) were set equal to 180° on the basis of the structural indications of ref 7 and 8 and of the high torsional barrier owing to the partial double-bond character (see ref 12, p 183).

The torsion angles ϑ_1 have been assigned possible values of ±90° on the basis of the structure of model compounds

0024-9297/87/2220-0293$01.50/0